A Study of Tidal Energy Dissipation and Bottom Stress in an Estuary

WENDELL S. BROWN AND RICHARD P. TRASK[1]

Department of Earth Sciences, University of New Hampshire, Durham NH 03824

(Manuscript received 31 March 1980, in final form 23 July 1980)

ABSTRACT

A method for inferring an area-averaged bottom stress and energy dissipation rate in a tidal estuarine channel is presented. The one-dimensional continuity and momentum relations are developed using simplifying assumptions appropriate for a well-mixed shallow and narrow estuary. The finite-difference form of these relations is derived for a section of the Great Bay Estuary, New Hampshire, an estuary which has been shown to have a relatively large energy dissipation rate. A set of current, bottom-pressure and sea-level measurements from the Estuary is used to estimate time series of all important first- and second-order terms in the momentum equation. Except near slack water, we find that the instantaneous first-order balance must be between the surface-slope-induced pressure gradient and bottom-stress forces. Important second-order contributions to the balance come from the inertial and convective acceleration terms. Time series of bottom stress are inferred by summing the estimated terms. For this study site the 14-day rms bottom stress is 45.1 ± 4.5 dyn cm^{-2} with a corresponding rms and mean dissipation rate of 3526 ± 420 and 2478 ± 297 ergs cm^{-2} s^{-1}, respectively. The role of the first-order tidal motion and nonlinearities in the mean second-order force balance is discussed.

1. Introduction

Based on the observed acceleration of the earth-moon system, Hendershott and Munk (1970) have calculated a tidal energy dissipation rate of 2.7×10^{19} ergs s^{-1} for the world's oceans. The inferred dissipation is likely to occur in the shallower regions of the oceans where the near-bottom velocity and hence frictional dissipation is greatest. Miller (1966) has estimated a dissipation rate of $1.7 \times 10^{19} \pm 50\%$ ergs s^{-1} for the coastal regions of the deep oceans and the shallow seas. The large uncertainty in this estimate is attributed to the relatively sparse set of current observations and a crude understanding of the frictional processes that lead to tidal energy dissipation.

Several attempts have been made to estimate the dissipation of tidal energy in specific coastal water bodies. One pioneering effort by Taylor (1919) was based on energy-budget considerations for the Irish Sea, where the net deficit of energy calculated for a tidal cycle was attributed to dissipation due to bottom friction plus work done by the Irish Sea on the moon. McLellan (1958) modified Taylor's method by also accounting for the energy required to mix the water column vertically, and he used the modified scheme to estimate dissipation due to friction in the Bay of Fundy. More recently, Garrett (1975) has shown that Taylor's method incorrectly considers the moon-sea interaction and thus the above estimates of the frictional dissipation inferred from Taylor/McLellan energy budgets are inaccurate.

Trask and Brown (1979) have corrected the Taylor method in accordance with Garrett's (1975) analysis and estimated a frictional dissipation rate of $1.6 \pm 0.1 \times 10^{14}$ ergs s^{-1} for the Great Bay Estuary, New Hampshire. This is to be compared with the dissipation estimate of $0.9 \pm 0.1 \times 10^{14}$ (Levine and Kenyon, 1975) for Narragansett Bay and a corrected dissipation estimate of 3.0×10^{17} ergs s^{-1} for the Bay of Fundy, respectively. Therefore, more tidal energy is dissipated in Great Bay than in Narragansett Bay, which has about 10 times more area. This difference is due to the more energetic tidal currents found in the estuaries bordering the Gulf of Maine.

Trask and Brown (1979) have shown that tidal energy dissipation in Great Bay Estuary (the Estuary henceforth) is due principally to bottom frictional processes. This is a particularly good estuary for this type of study because the effects of density gradients and wind stress are small compared to those of tidal forcing at the mouth. In this paper we explore the relation among the tidal hydrodynamics, the bottom stress and the energy dissipation. Smith and McLean (1977) discuss some of the difficulties in making local estimates of bottom stress from boundary-layer flow measurements in a natural channel

[1] Present affiliation: Woods Hole Oceanographic Institution, Woods Hole, MA 02543.

0022-3670/80/111742-13$07.25

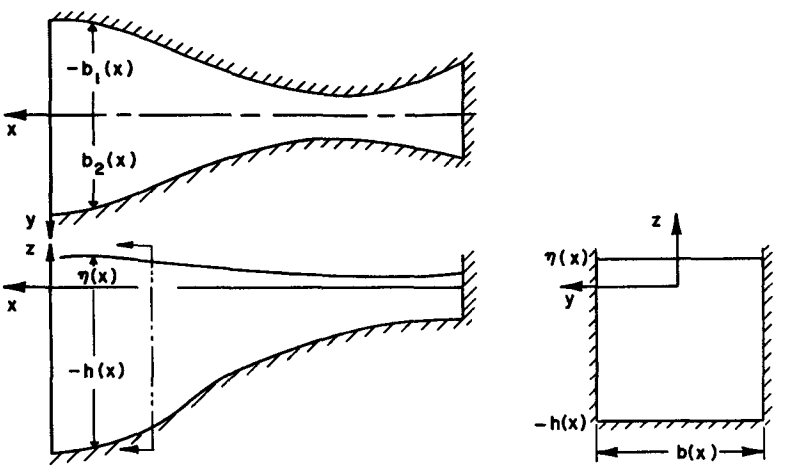

FIG. 1. Schematic diagrams of a rectangular section estuary.

with variable bottom topography. In addition, there are unresolved difficulties in the hydrodynamic interpretation of a few individual estimates of local bottom stress. In this paper we avoid some aspects of this problem by inferring total bottom stress from the equations of motion. Bowden *et al.* (1959) have had some limited success in using the two-dimensional momentum equation to estimate the vertical distribution of stress and eddy viscosity. Here we describe a procedure for the "dynamic inference" of an area-averaged bottom stress using the one-dimensional (cross-section averaged) continuity and momentum equations, which are developed in Section 2, and field measurements, which are described in Section 3. A discussion of the stress and dissipation estimates appears in Section 4.

2. Theoretical considerations

The following is a theoretical development concerning tidal dynamics in a narrow and shallow estuarine channel shown in Fig. 1. We will consider the case for which sea level fluctuations η are small compared to depth h. Thus the tidal, density-driven and wind-driven problems are linearly related and can be treated separately. The dynamics will be expressed in terms of cross-section-averaged velocity $U(x)$, surface elevation $\eta(x)$, depth $h(x)$ and cross-section area $A(x)$; therefore we begin with the vertically and horizontally integrated form of the continuity equation for a channel of arbitrary cross section, i.e.,

$$\frac{\partial \tilde{u}}{\partial x} + \frac{\partial\{\eta + h\}}{\partial t} = 0, \qquad (1)$$

where the tilde and braces denote the integrals

$$\int_{-b_1}^{b_2}\int_{-h}^{\eta} \cdots dzdy \quad \text{and} \quad \int_{-b_1}^{b_2} \cdots dy,$$

respectively. Here we have assumed that velocities normal to solid boundaries are zero. Since in general $A = \{\eta + h\}$ and $\tilde{u} = AU$ then (1) can be written

$$\frac{\partial A}{\partial t} + \frac{\partial AU}{\partial x} = 0. \qquad (2)$$

For discussion of the more restrictive case of a rectangular channel of width $b = b_1 + b_2$, we define the lateral average (using double overbars) as

$$\frac{1}{b}\int_{-b_1}^{b_2} \cdots dy,$$

so that $\overline{\overline{(\eta + h)}} = b^{-1}\{\eta + h\}$. Thus since h is independent of time we can rewrite (1) as

$$\frac{\partial \bar{\bar{\eta}}}{\partial t} + \frac{1}{b}\frac{\partial(AU)}{\partial x} = 0. \qquad (3)$$

The x-momentum equation of interest is

$$\frac{\partial u}{\partial t} + u\frac{\partial u}{\partial x} + v\frac{\partial u}{\partial y} + w\frac{\partial u}{\partial z} - fv = -\frac{1}{\rho}\frac{\partial p}{\partial x} + \frac{1}{\rho}\frac{\partial \tau_x}{\partial z} + \frac{1}{\rho}\frac{\partial \tau_x}{\partial y}, \qquad (4)$$

where $\mathbf{v}(u,v,w)$ is velocity, $p = \rho g(\eta - z)$ is assumed to be hydrostatic pressure, τ_x is x-directed stress, and ρ is density, which is assumed to be constant. By adding $u(\nabla\cdot\mathbf{v})$ to (4) and collecting terms we have

$$\frac{\partial u}{\partial t} + \frac{\partial u^2}{\partial x} + \frac{\partial uv}{\partial y} + \frac{\partial uw}{\partial z} - fv = -\frac{1}{\rho}\frac{\partial p}{\partial x} + \frac{1}{\rho}\frac{\partial \tau_x}{\partial z} + \frac{1}{\rho}\frac{\partial \tau_x}{\partial y}. \quad (5)$$

When we integrate twice,

$$\frac{1}{A}\int_{-b_1}^{b_2}\int_{-h}^{\eta} \cdots dzdy,$$

while applying boundary conditions

$$w(\eta) = D\eta/Dt, \quad w(-h) = D(-h)/Dt,$$

$$V(b_2) = U(b_2)\partial b_2/\partial x, \quad v(b_1) = U(-b_1) - \partial b_1/\partial x$$

at the surface, bottom and two vertical sidewalls, and make a liberal use of Leibnitz's rule Eq. (5) becomes

$$\frac{1}{A}\frac{\partial \tilde{u}}{\partial t} + \frac{1}{A}\frac{\partial u^2}{\partial x} - \frac{f}{A}\tilde{v} = -\frac{g}{A}\left\{\left[(\eta + h) - \frac{p(\eta)}{\rho g}\right]\frac{\partial \eta}{\partial x}\right\} + \frac{1}{\rho A}\left\{\tau_s\left(1 + \frac{\partial \eta}{\partial x}\right) - \tau_b\left(1 - \frac{\partial(-h)}{\partial x}\right)\right\} + \frac{1}{\rho A}\overline{(\tau_x|_{b_2} - \tau_x|_{b_1})}, \quad (6)$$

where $p(\eta)$ and τ_s are the surface pressure and stress, τ_b is the bottom stress, and $\overline{\tau_x|_{b_2}}$ and $\overline{\tau_x|_{b_1}}$ are the vertical integrals of sidewall stress. Here the single overbar defines the integral $\int_h^{\eta} \cdots dz$. Manipulating the definitions of U and A it can be shown that

$$\frac{1}{A}\frac{\partial \tilde{u}}{\partial t} = \frac{\partial U}{\partial t} + U\frac{\partial U}{\partial x} - \frac{1}{A}\frac{\partial}{\partial x}\left(\frac{1}{A}\tilde{u}^2\right). \quad (7)$$

Thus (6) on substitution of (7) becomes

$$\frac{\partial U}{\partial t} + U\frac{\partial U}{\partial x} = -\frac{g}{A}\left\{\left[(\eta + h) - \frac{p(\eta)}{\rho g}\right]\frac{\partial \eta}{\partial x}\right\} + \frac{1}{\rho A}\left\{\tau_s\left(1 - \frac{\partial \eta}{\partial x}\right) - \tau_b\left(1 - \frac{\partial(-h)}{\partial x}\right)\right\} + \frac{1}{\rho A}\overline{(\tau_x|_{b_2} - \tau_x|_{-b_1})} + \frac{f}{A}\tilde{v} - \frac{1}{A}\frac{\partial}{\partial x}(\widetilde{u^2} - \tilde{u}^2). \quad (8)$$

(a) (b) (c) (d) (e)

This relation can be simplified by assuming that the following terms are very small compared to others in the equation: (i) $p(\eta) \ll \rho g h$; (ii) $\tau_s \ll \tau_b$; (iii) $\partial h/\partial x \ll 1$; (iv) Kelvin number $\equiv fb/\sqrt{gh} \ll 1$; (v) horizontal aspect ratio $\equiv h/b \ll 1$; and (vi) $\widetilde{u^2}/\tilde{u}^2 \ll 1$. For the Estuary, assumptions (i)–(iii) are valid and thus terms (a) and (b) in (8) are simplified as shown below. For a narrow estuary in which the width-to-length ratio is very small, the Kelvin number is small and the cross-channel geostrophic balance is set up much more rapidly than changes in axial flow. Thus Coriolis effects are unimportant and term (d) of (8) can be neglected. In the Estuary $h/b = 0.002 \ll 1$ and therefore lateral stresses, which scale as h, are less important than bottom stresses, which scale as b, and thus term (c) can be neglected. Finally, Johns (1978) has shown numerically that assumption (vi) is true for an estuarine channel similar to the one considered here.

Therefore, Eq. (8) can be rewritten

$$\frac{\partial U}{\partial t} + U\frac{\partial U}{\partial x} = -\frac{g}{A}\left\{(\eta + h)\frac{\partial \eta}{\partial x}\right\} - \frac{1}{\rho A}\{\tau_b\}. \quad (9)$$

The pressure-gradient term of (9) can be simplified further with the additional assumption (vii) $\eta/h \ll 1$ in which case $A \approx hb$. In this case

$$-\frac{g}{A}\int_{-b_1}^{b_2}\left[(\eta + h)\frac{\partial \eta}{\partial x}\right]dy \approx -\frac{g}{b}\int_{-b_1}^{b_2}\frac{\partial \eta}{\partial x}dy \quad (10)$$

and, furthermore, the right-hand side of (10) can be written

$$-g\left[\frac{\partial}{\partial x}\frac{1}{b}\int_{-b_1}^{b_2}\eta dy + \frac{\partial b}{\partial x}\frac{1}{b^2}\int_{-b_1}^{b_2}\eta dy - \frac{\eta(b_2)}{b}\frac{\partial b_2}{\partial x} + \frac{\eta(-b_1)}{b}\frac{\partial(-b_1)}{\partial x}\right].$$

(a) (b) (c) (d)

For small cross-channel elevation differences, such that $\delta\eta/\eta \ll 1$, terms (b) + (c) + (d) ≈ 0. Thus, the pressure gradient term in (9) is

$$-\frac{g}{A}\left\{(\eta + h)\frac{\partial \eta}{\partial x}\right\} \approx -g\frac{\partial \bar{\eta}}{\partial x} \quad (11)$$

and (9) can be approximated as

$$\frac{\partial U}{\partial t} + U\frac{\partial U}{\partial x} = -g\frac{\partial \bar{\eta}}{\partial x} - \frac{\bar{\tau}_b}{\rho h}. \quad (12)$$

Note that (12) is in error by the omission of the term $-g/A\ \overline{\eta\partial\eta/\partial x}$; a point that will be explored later.

Consider the application of (3) and (12) to the case of a tidal wave with amplitude, frequency and wavenumbers of a_0, σ and $k = 2\pi/\lambda$ in an estuary of con-

stant depth h whose characteristic length scale L_0 is much less than the tidal wavelength λ. For the case of a uniform-width channel L_0 is the estuary length; otherwise L_0 is the characteristic width-variability scale. To explore the relative importance of the terms in (3) and (12), we scale the variables as follows:

$$\bar{\eta} = a_0\hat{\eta}, \quad U = U_0\hat{u}, \quad x = L_0\hat{x},$$
$$t = \sigma^{-1}\hat{t} \quad \text{and} \quad \bar{\tau}_b = \rho C_D U_0^2 \hat{\tau}_b,$$

where C_D is a dimensionless bottom drag coefficient ($\sim 10^{-3}$) and the caret identifies nondimensional O(1) variables. Spatial variations in $\bar{\eta}$, U and b, which are scaled with $\delta\eta$, δU and δb, respectively.

It is informative to rewrite the continuity equation as

$$A\frac{\partial U}{\partial x} = -b\frac{\partial \bar{\eta}}{\partial t} - U\frac{\partial A}{\partial x} \qquad (13)$$
$$\text{(a)} \qquad \text{(b)}$$

to show how the divergence of the transport on the left-hand side of (13) is related to wave and geometry effects of terms (a) and (b), respectively on the right-hand side of (13). The scaled form of (13) becomes

$$\frac{\partial \hat{u}}{\partial \hat{x}} = -\left[\left(\frac{a_0}{h}\right)\left(\frac{\sigma L_0}{\delta U}\right)\frac{\partial \hat{\eta}}{\partial \hat{t}} + \left(\frac{\delta b}{b}\right)\left(\frac{U_0}{\delta U}\right)\hat{u}\frac{\partial \hat{b}}{\partial \hat{x}}\right] \qquad (14)$$

and the corresponding scaled form of (12) becomes

$$\frac{\partial \hat{u}}{\partial \hat{t}} + \left(\frac{\delta U}{\sigma L_0}\right)\hat{u}\frac{\partial \hat{u}}{\partial \hat{x}} = -\left(\frac{g\delta\eta}{\sigma U_0 L_0}\right)\frac{\partial \hat{\eta}}{\partial \hat{x}} - \left(\frac{C_D U_0}{\sigma h}\right)\hat{\tau}_b. \qquad (15)$$

a. Uniform-width channel

It is clear from (14) that for a uniform-width channel ($\delta b \equiv 0$) and for $\eta/h \ll 1$, Eq. (3) can be approximated by

$$\frac{\partial \bar{\eta}}{\partial t} + h\frac{\partial U}{\partial x} = 0. \qquad (16)$$

In addition, (14) shows that $\delta U = a_0\sigma L_0/h$. But $\sigma = k(gh)^{1/2}$ so that

$$\delta U = a_0\left(\frac{g}{h}\right)^{1/2} L_0 k = U_0 L_0 k, \qquad (17)$$

where $U_0 = a_0(g/h)^{1/2}$ is the progressive wave velocity scale.

If we scale $\delta\eta$ likewise as $L_0 k a_0$ then (15) can be rewritten as

$$\frac{\partial \hat{u}}{\partial \hat{t}} + \left(\frac{U_0}{(gh)^{1/2}}\right)\hat{u}\frac{\partial \hat{u}}{\partial \hat{x}} = -\left(\frac{(gh)^{1/2}}{U_0}\right)\left(\frac{a_0}{h}\right)\frac{\partial \hat{\eta}}{\partial \hat{x}} - \left(\frac{C_D}{hk}\frac{U_0}{(gh)^{1/2}}\right)\hat{\tau}_b. \qquad (18)$$

Upon substitution of typical Estuary values of $U_0 = 1$ m s^{-1}, $a_0 = 1$ m, $h = 10$ m and $\sigma/k = (gh)^{1/2} \sim 10$ m s^{-1} Eq. (18) becomes

$$\frac{\partial \hat{u}}{\partial \hat{t}} + (10^{-1})\hat{u}\frac{\partial \hat{u}}{\partial \hat{x}} = -\frac{\partial \hat{\eta}}{\partial \hat{x}} - \hat{\tau}_b. \qquad (19)$$

Therefore, for $\delta_b \equiv 0$ the approximate form of (12) is

$$\frac{\partial U}{\partial t} = -g\frac{\partial \bar{\eta}}{\partial x} - \frac{\bar{\tau}_b}{\rho h}. \qquad (20)$$

b. Variable-width channel

For the more realistic case of a constant-depth and variable-width channel, in which δb varies on spatial scales of L_0, the δU scale can be determined from the continuity form (14). In particular, for the Estuary, where $\delta b/b \geq 10^{-1}$ over scales $L_0 = 10^3$ m and the other scales are as above, the first-order balance is between the $\partial\hat{u}/\partial\hat{x}$ and $\hat{u}\,\partial\hat{b}/\partial\hat{x}$ terms which means δU scales as $U_0\delta b/b$. Thus, Eq. (3) can be approximated by

$$\frac{\partial U}{\partial x} + \frac{U}{b}\frac{\partial b}{\partial x} = 0. \qquad (21)$$

Using the same δU scaling the momentum equation (15) becomes

$$\frac{\partial \hat{u}}{\partial \hat{t}} + \left(\frac{U_0}{\sigma L_0}\right)\left(\frac{\delta b}{b}\right)\hat{u}\frac{\partial \hat{u}}{\partial \hat{x}} = -\left(\frac{g\delta\eta}{\sigma U_0 L_0}\right)\frac{\partial \hat{\eta}}{\partial \hat{x}} - \left(\frac{C_D U_0}{\sigma h}\right)\hat{\tau}_b. \qquad (22)$$

At this point the scaling for $\delta\eta$ is undetermined because the wave-scaling $L_0 k a_0$ is no longer appropriate. We could choose to scale $\delta\eta$ in terms of the bottom stress but rather we choose to find a balance in terms of the convective term $U\delta U/\delta x$, whose effect is going to become dominant as $\delta b/b$ increases. In a form that more nearly corresponds to δU scaling we find that $\delta\eta$ scales as $(U_0^2/g)(\delta b/b)$. Eq. (22) then becomes

$$\frac{\partial \hat{u}}{\partial \hat{t}} + \left(\frac{U_0}{\sigma L_0}\right)\left(\frac{\delta b}{b}\right)\hat{u}\frac{\partial \hat{u}}{\partial \hat{x}} = -\left(\frac{U_0}{\sigma L_0}\right)\left(\frac{\delta b}{b}\right)\frac{\partial \hat{\eta}}{\partial \hat{x}} - \left(\frac{C_D U_0}{\sigma h}\right)\hat{\tau}_b. \qquad (23)$$

Thus for $\delta b/b = 10^{-1}$ and other values as used above, Eq. (23) becomes

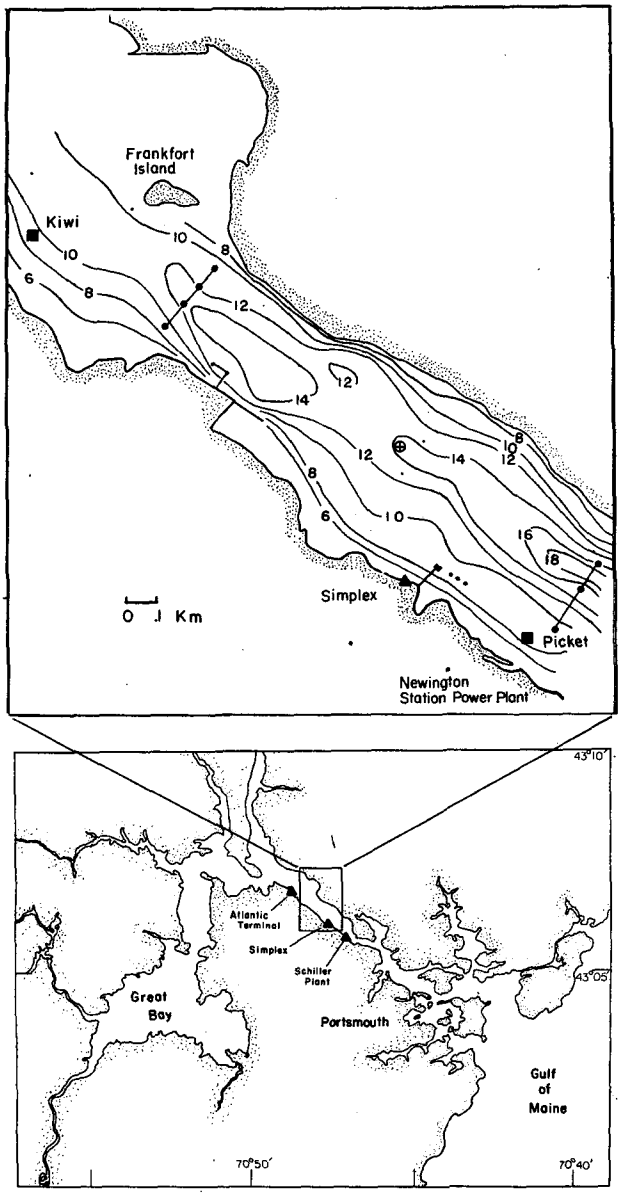

FIG. 2. The Great Bay Estuary and the area of interest in the 1978 field program. Locations of the NOS tide stations (▲), the transect station locations (●), the current-meter location (⊕) and the pressure-instrument locations (■) Kiwi and Picket are shown. The depth contours are in meters relative to mean low water (MLW).

$$\frac{\partial \hat{u}}{\partial \hat{t}} + \hat{u}\frac{\partial \hat{u}}{\partial \hat{x}} = -\frac{\partial \hat{\eta}}{\partial \hat{x}} - \hat{\tau}_b, \qquad (24)$$

which shows that for even small channel-width variations all terms can be equally important.

For $\delta b/b = O(10^{-1})$ the appropriate dimensional momentum equation is

$$\frac{\partial U}{\partial t} + U\frac{\partial U}{\partial x} = -g\frac{\partial \bar{\bar{\eta}}}{\partial x} - \frac{\bar{\bar{\tau}}_b}{\rho h}. \qquad (25)$$

We seek a finite-difference form of (25) with which to compare observations. It is found by integrating from the upstream transect at x_1 to the downstream transect at x_2:

$$\frac{1}{(x_2 - x_1)}\left[\int_{x_1}^{x_2}\frac{\partial U}{\partial t}dx + \int_{x_1}^{x_2}\frac{\partial (U^2/2)}{\partial x}dx\right] = \frac{-g}{(x_2 - x_1)}\left[\int_{x_1}^{x_2}\frac{\partial \bar{\bar{\eta}}}{\partial x}dx + \frac{1}{\rho h}\int_{x_1}^{x_2}\bar{\bar{\tau}}_b dx\right].$$

This reduces to

$$\frac{\delta\langle U\rangle}{\delta t} + \frac{\delta(U^2/2)}{\delta x} = -g\frac{\delta\eta}{\delta x} - \frac{\langle\tau_b\rangle}{\rho h}, \qquad (26)$$

where $\delta x = x_2 - x_1$, $\delta(U^2/2)$ and $\delta\eta$ are the differences $U(x_2)^2 - U(x_1)^2$ and $\bar{\bar{\eta}}(x_2) - \bar{\bar{\eta}}(x_1)$, respectively, and angle braces indicate a study-site spatial average. Thus, using a rearranged form of (26), the space-averaged bottom stress can be determined using estimates of the other terms according to

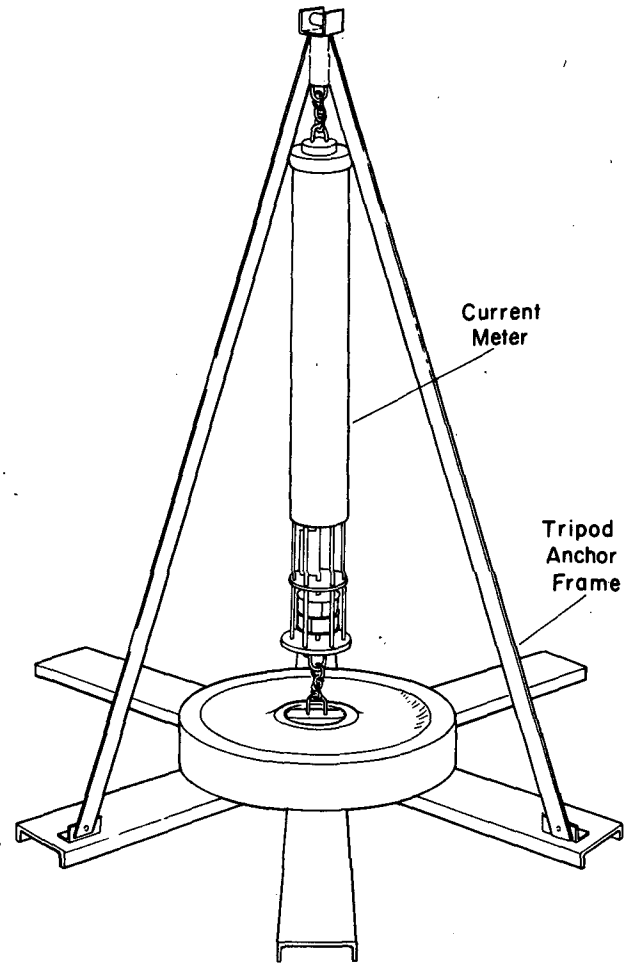

FIG. 3. A schematic drawing of the tripod anchor frame used to secure the Geodyne current meter in the center of the channel.

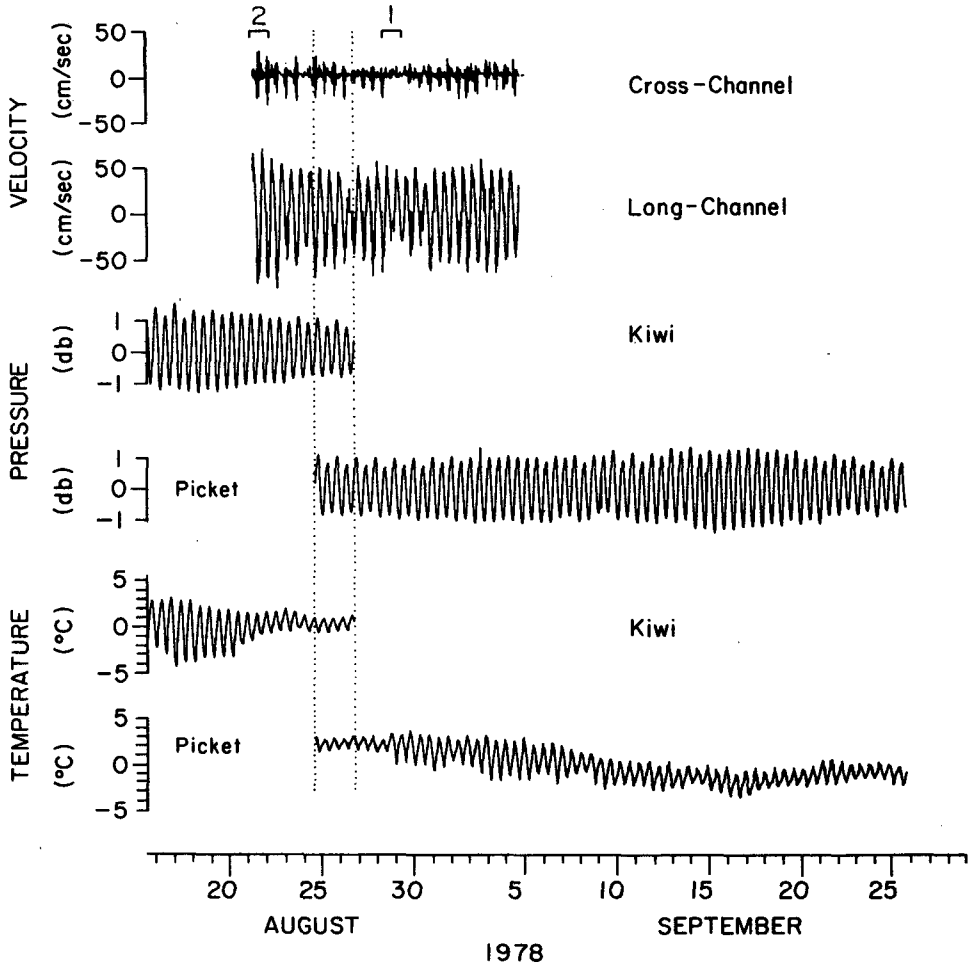

FIG. 4. A summary of data acquisition during the 1978 field program. The times of the 13-h downstream (2) and upstream (1) transects are indicated as well as the 2-day overlap period of the pressure and current measurements. The mean values have been removed from the temperature and pressure series.

$$\langle \tau_b \rangle = -\rho h \left(\frac{\delta \langle U \rangle}{\delta t} + \frac{\delta (U^2/2)}{\delta x} + g \frac{\delta \eta}{\delta x} \right). \quad (27)$$

(a) (b) (c) (d)

The corresponding finite difference form of (20) for a uniform width channel is

$$\langle \tau_b \rangle = -\rho h \left(\frac{\delta \langle U \rangle}{\delta t} + g \frac{\delta \eta}{\partial x} \right). \quad (28)$$

3. Field program

A field program was designed to provide estimates of the terms in (27) in a region of the Great Bay Estuary, New Hampshire. A 2 km section of the Estuary shown in Fig. 2 was selected for the study because of its relatively high currents and uniform geometry. Previous observations described by Swenson *et al.* (1977) and Silver and Brown (1979) show that the properties of the Estuary at this location are sufficiently uniform throughout the tidal cycle that a constant density approximation is reasonable.

In order to estimate $\delta\eta/\delta x$, a pair of internally recording instruments using Paroscientific Digiquartz pressure sensors and thermistors was deployed on the 10 m isobath as shown in Fig. 2. A thermistor record was used to correct for the temperature sensitivity of the pressure sensor. These pressure sensors have short-term precisions better than 1 mm and long-term stability of about 1 cm per month. Because of the uncertainty in the depth of each instrument, however, the mean value of $\delta\eta/\delta x$ cannot be measured and has been assumed to be zero. This assumption is consistent with the very low ratio of river flow to tidal prism of 1:640 found for this estuary by Arellano (1978).

A set of current-profile and moored-current meas-

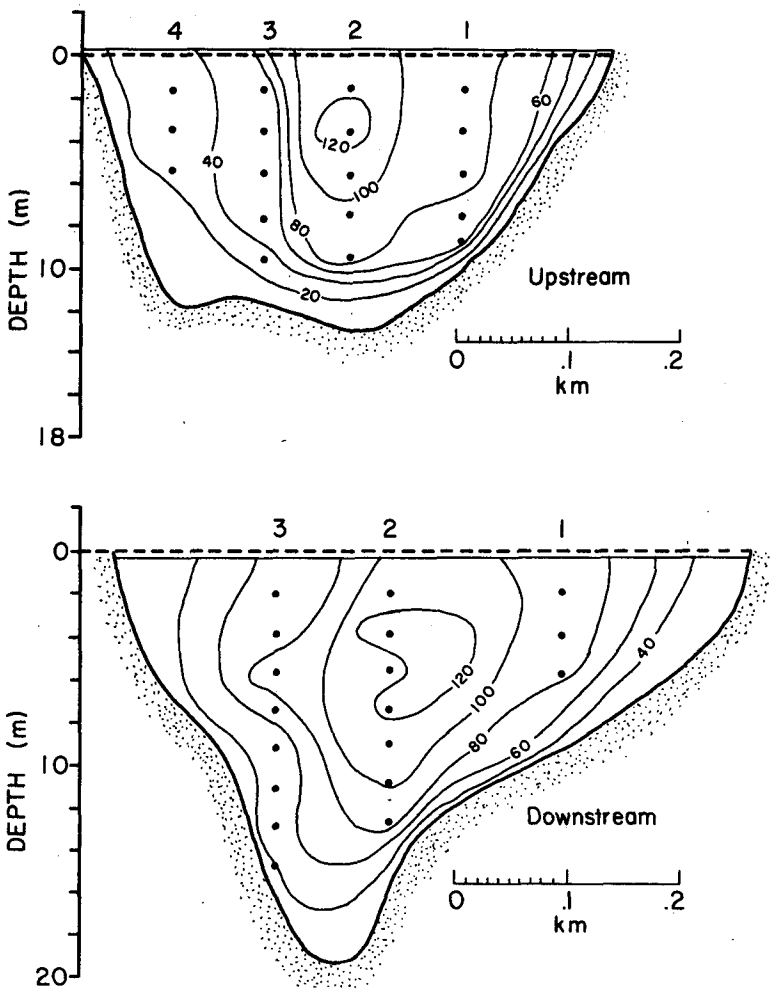

FIG. 5. A seaward view of typical sections of longitudinal current at the upstream and downstream transects of the study area. Ebb or seaward currents are positive. Contour interval is 20 cm s^{-1}, dashed horizontal line indicates mean low water, solid line indicates the water surface and the circles indicate the locations of current measurements.

urements was made for purposes of estimating the current and current-derivative terms in (27). Currents were sampled at 10 min intervals by a single Geodyne 102 film-recording current meter, which was deployed for about a month in a configuration as shown in Fig. 3 at the location shown in Fig. 2. The rotor height was restricted to 75 cm above the bottom at this center-channel location to avoid interference with the deep-draft oil tanker traffic in this section of the Estuary. In addition to the moored current measurements, a series of current profiles was measured with a Marsh and McBirney electromagnetic current meter at the two transects indicated on Fig. 2 and at the current-meter site. The purpose of the profile measurements was to determine the relations between the moored current observations and the section-averaged currents at the three sites. At the outset we assumed that the relationships between the different current measurements determined for a single tidal cycle would be applicable for other times.

4. Results

A summary of the moored-instrument data acquisition during the summer 1978 field study is shown in Fig. 4. Originally the study was to consist of one month of overlapping records but a variety of instrumentation problems led to the reduced length of records shown. The 2-day overlap of the pressure and current records, which is used in the analysis to follow, is indicated, along with the days during which the current transects were made. Clearly, the tides are dominant in all of the observed records.

a. Dynamic inferrence of bottom stress

The section-averaged currents, which are used to estimate the velocity gradient term $\delta U/\delta x$, were determined from the transport estimates for the upstream and downstream transects. A 13 h series of transport values has been estimated at each transect from current maps like those shown in Fig. 5. The current-profile measurements were made near neap tide for the upstream section and near spring tide for the downstream section, with tidal ranges of 1.50 and 2.94 m, respectively. These transport estimates were normalized to the mean tidal range of 2.00 m and are compared in Fig. 6. The diurnal inequality is evident in these pictures of ebb and flood transport. A comparison of the time-integrated transports with known estimates of tidal-prism volumes (see Trask and Brown, 1979) indicates that this method underestimates the actual transport by about 10%, on account of failure to account properly for current on the flanks of the channel. Therefore, we have amplified our estimates by that percentage.

The relation between the moored currents and transports at the upstream and the downstream transects has been determined from the calculated regressions only (Fig. 7) because there was no significant phase lag between the observations. The zero intercept of the regression was fortuitous. Because tidal flow dominates the kinematics and dynamics in the Estuary we have assumed that the calculated regressions between moored and transect-

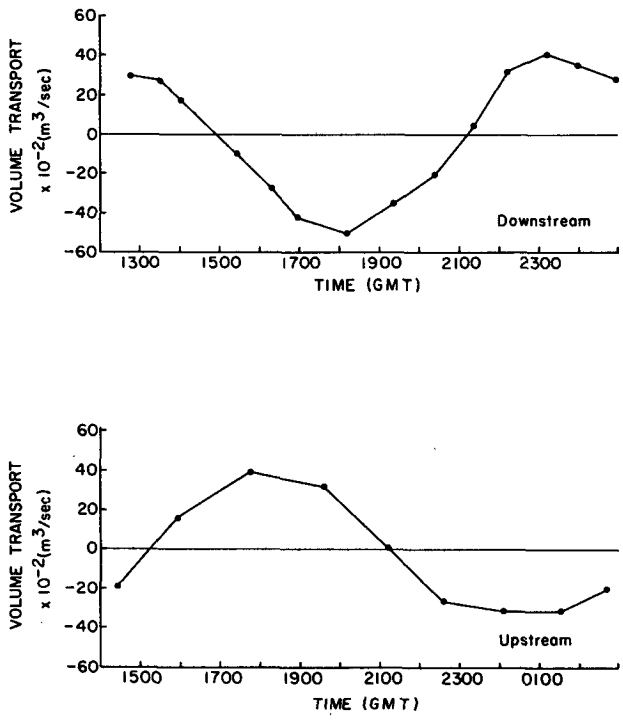

FIG. 6. Time series of the normalized volume transports (see text) at the upstream and downstream transects. The upper plot (a) shows downstream transport data collected on 22 August 1978, and the lower plot (b) shows upstream transport data collected on 29 August 1978.

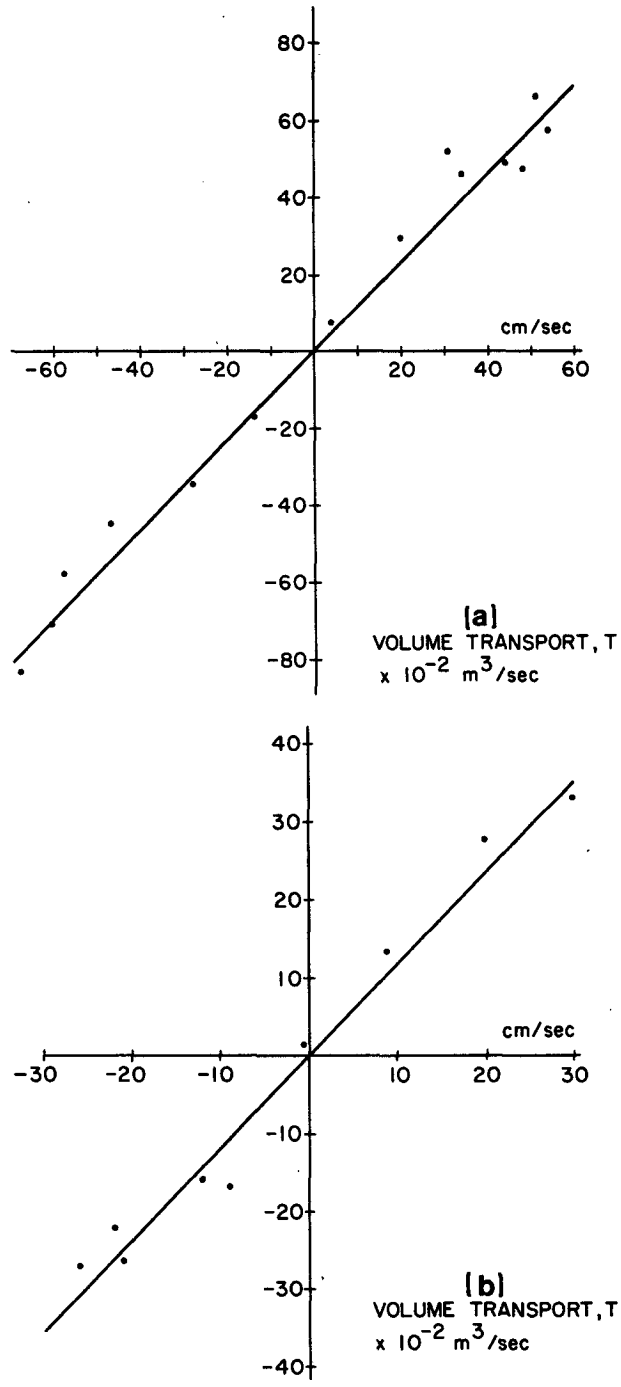

FIG. 7. (a) The longitudinal current (x) versus upstream-transect transport (y). The linear best fit of the data is $y = 116.9x$ with a corresponding r-square value of 0.975. (b) The longitudinal current (x) versus downstream-transect transport (y). The linear best fit of the data is $y = 114.2x$ with a corresponding r-square value of 0.981.

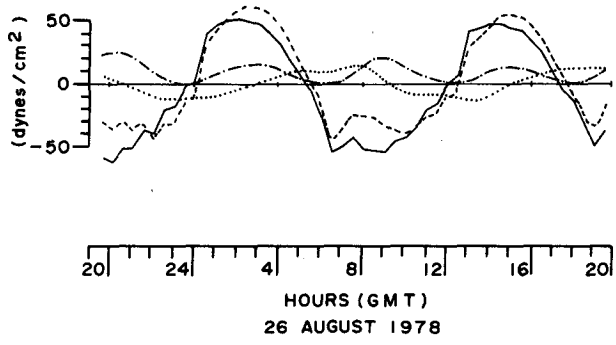

FIG. 8. A comparison of the inertial (dotted), convective-acceleration (dot-dashed) and pressure-gradient-term (solid) [see (27) in text] contributions to the bottom stress τ_b (dashed) over a diurnal tidal cycle. Except near slack water, where $\delta\eta/\delta x$ is zero, the principal balance is between the pressure-gradient and bottom-stress terms.

averaged currents are approximately true at all times. Thus we have been able to calculate $\langle U \rangle$ and δU^2 for times other than those of the observed transports.

These data have been used to estimate the individual terms in (27), which are compared for one tidal cycle in Fig. 8. The pressure gradient term $g\delta\eta/\delta x$ is estimated from the difference between Picket and Kiwi bottom pressure. The inertial term $\delta\langle U\rangle/\delta t$ has been calculated by first differencing the 10 min values of $\langle U \rangle$ and filtering out frequencies about 3 cph. We justify this procedure because we are principally interested in the tidal dynamics and much of the high-frequency variability in the observed acceleration was found to be spurious, as discussed by Trask and Brown (1979). The convective acceleration term $\delta(U^2/2)\delta x$ was calculated from the transport estimates at each transect. With the exception of periods near slack water, when $\delta\eta/\delta x$ is small, the principal dynamic balance is between the bottom stress and the pressure gradient. A smaller order contribution to that balance is due to convective and inertial accelerations (see Fig. 8). These results are summarized in Table 1.

In order to explore the spring through neap tide variability in the bottom stress, a 14-day series of the terms in (27) was calculated with the current-related terms computed as before and a pressure-gradient term now based on predicted sea levels. The stress series and its component terms are shown in Fig. 9, and the rms values are compared with the 2-day results in Table 1. A synthetic pressure gradient term was used because the required data were not available (see Fig. 4). The sea level predictions are based on the tidal-harmonic analysis of sea level measurements made by the National Ocean Survey and the University of New Hampshire during a 1975 field program described by Swenson *et al.* (1977). Trask and Brown (1979) describe how the pressure-

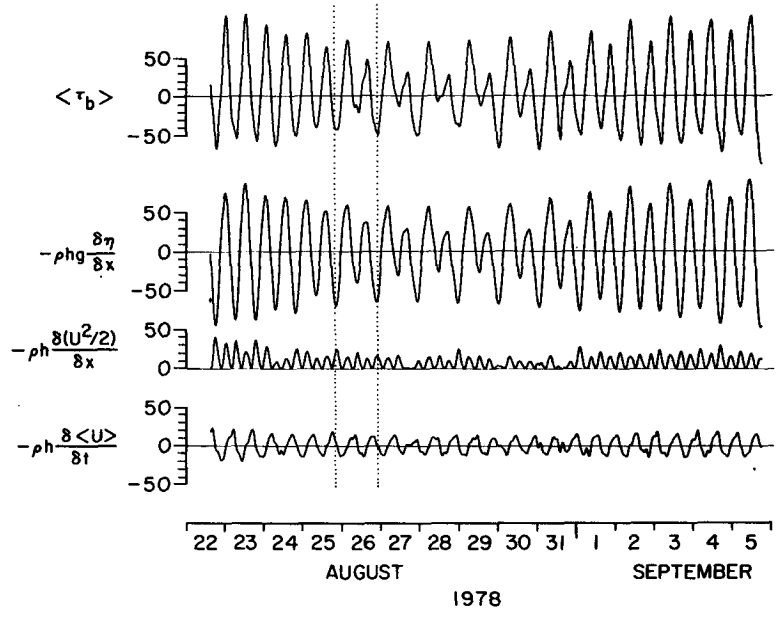

FIG. 9. A 14-day comparison of the bottom-stress term $\langle \tau_b \rangle$ with the components from which it was formed in accordance with Eq. (27). The inertial and convective-acceleration terms were formed in the manner described in the text with measured currents, and the pressure-gradient term was estimated from predicted sea levels. The spring neap tidal cycle is clearly apparent in these results. See Fig. 8 for the relative phase of the different components during the period indicated by the dotted lines. The units of all terms are in dyn cm^{-2} and times are GMT.

TABLE 1. The rms and mean values of the component terms in (27) are shown in units of dyn cm^{-2} for the 1-, 2- and 14-day averaging periods discussed in the text. The corresponding rms and mean values of the study area averaged dissipation $\langle\phi\rangle$ in units of ergs cm^{-2} s^{-1} are also included.

Average period	$-\rho gh\frac{\delta\eta}{\delta x}$		$-\rho h\frac{\delta(U^2/2)}{\delta x}$		$-\rho h\frac{\delta\langle U\rangle}{\delta t}$		$\langle\tau_b\rangle$		$\langle\phi\rangle$	
	rms	Mean	rms	Mean	rms	Mean	rms	Mean	rms	Mean
1	39.1 ± 2.0	—	10.9 ± 1.3	8.4 ± 1.0	9.3 ± 0.5	−0.3 ± 0.5	36.3 ± 3.6	8.1 ± 0.8	2525	2021 ± 243
2	36.8 ± 1.8	—	9.7 ± 1.2	7.1 ± 0.9	8.3 ± 0.4	−0.2 ± 0.5	33.7 ± 3.4	7.0 ± 0.7	2236	1696 ± 203
14	47.8 ± 2.4	—	11.6 ± 1.4	8.5 ± 1.0	9.7 ± 0.5	0.1 ± 0.5	45.1 ± 4.5	7.8 ± 0.8	3526	2478 ± 297

gradient estimate was computed from the predicted sea levels at Atlantic Heights, Simplex and the Schiller Power Plant (see Fig. 2). The calculated rms bottom stresses $\langle\tau_b\rangle$ for the observed and synthetic pressure gradients for the one day period indicated in Fig. 9 are 36.3 ± 3.6 and 35.3 ± 3.5 dyn cm^{-2}, respectively. Thus, we conclude that bottom stress computed on the basis of predicted data is a good approximation of the observed-data computation.

In summary, the results above show that for a relatively straight section of this well-mixed tidal estuary the bottom stress can be estimated to within 20% using sea level measurements alone. Furthermore the estimate can be improved by correcting for the contribution of the convective-acceleration term, which can be estimated from the channel geometry and the tidal prism volume. The resultant stress estimated, using this dynamical-inference method, can be interpreted as a bottom stress which is spatially averaged over the region of the measurements.

b. Dissipation

The tidal energy dissipation has been calculated in accordance with the relation $\langle\phi\rangle = \langle\tau_b\rangle\langle U\rangle$, which is the study-area-averaged dissipation rate per unit area. An example of that calculation for the 1-day results (see Fig. 8) is displayed in Fig. 10, which shows a comparison of the component terms $\langle\tau_b\rangle$ and $\langle U\rangle$ and the dissipation $\langle\phi\rangle$. (The nonzero values are probably related to the uncertainties in our estimates of $\langle U\rangle$ and $\langle\tau_b\rangle$.) Thus, as expected, we find an oscillating dissipation with a nonzero mean of 2021 ± 243 ergs cm^{-2} s^{-1} in this case. A value of 2478 ± 297 ergs cm^{-2} s^{-1} was found for the 14-day calculation, which correctly averages the

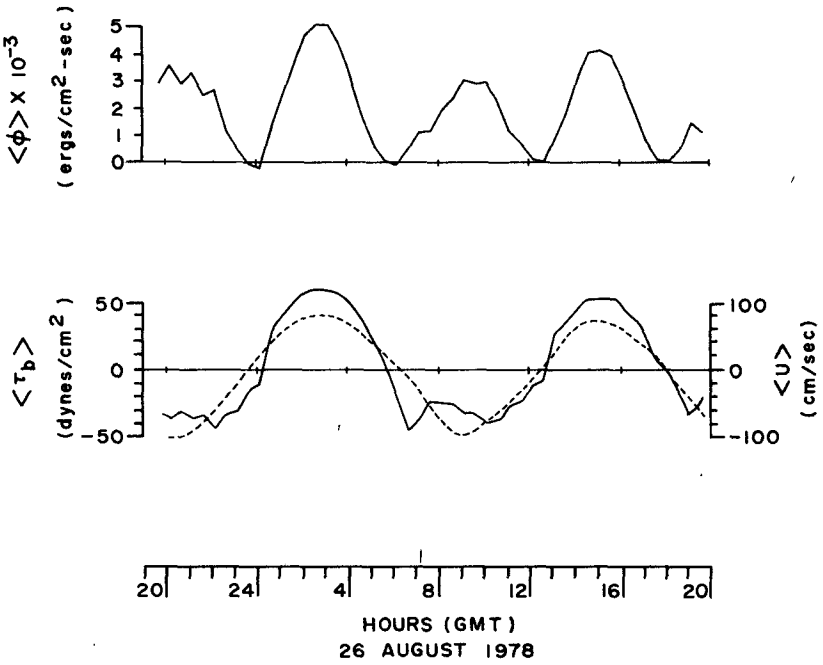

FIG. 10. Tidal energy dissipation, $\langle\phi\rangle = \langle\tau_b\rangle\langle U\rangle$ for the one-day results (see Fig. 8) is compared with the component terms $\langle\tau_b\rangle$ (solid) and $\langle U\rangle$ (dashed) below.

spring neap tidal effects. (The bias introduced by the longer period tidal components is much smaller.)

Using the same data set presented here and the corrected Taylor method, Trask (1979) has calculated a study-area averaged dissipation rate of 4940 ± 2519 ergs cm^{-2} s^{-1}. These two methods provide results that barely agree within the uncertainty limits of both. The large uncertainty limits associated with the Taylor calculation are associated with difficulty in differencing the very large transport values at the upstream and downstream transects. This source of uncertainty is not nearly so important for the dynamical inference method because the convective acceleration term, which depends on such a difference, is small. Therefore, we have reason to be more confident in the lower number.

5. Discussion

a. Dynamical balances

The results presented above clearly show that the *first-order* instantaneous force balance in the study area is between the bottom-stress and pressure-gradient forces if the assumptions underlying (27) are satisfied in the Estuary. The assumptions leading to (9) are satisfied, but since $\eta/h \approx 0.2$ and h is not constant, the assumptions leading to (27) are not strictly satisfied. Thus the magnitude of the errors introduced by these violations must be examined.

From (10) the error term ϵ_η associated with the assumption $\eta/h \ll 1$ is

$$\epsilon_\eta = -(\rho hg/A)\int_{-b_1}^{b_2} \eta(\partial\eta/\partial x)dy,$$

where $A \approx bh$, $\bar{\eta} \approx a\cos\sigma t$, $\overline{\overline{\partial\eta/\partial x}} \approx c\sin\sigma t$ with $a = 100$ cm and $c = 5 \times 10^{-5}$. Thus

$$\text{rms } \epsilon_\eta \sim \rho g \text{ rms } (\bar{\eta}\overline{\overline{\partial\eta/\partial x}}) = \rho g(ac/2\sqrt{2}) = 1.77 \text{ dyn cm}^{-2},$$

which is small even in comparison with the *second-order* inertial and convective acceleration effects (see Table 1), and can therefore be neglected.

If we had not assumed that h = constant, then (27) would have been

$$\left\langle \frac{\tau_b}{\rho h} \right\rangle = \frac{\delta\langle u\rangle}{\delta t} + \frac{\delta(U^2/2)}{\delta x} + g\frac{\delta\eta}{\delta x}.$$

To determine the error incurred by assuming h = constant we find a Taylor series expansion of

$$\langle\rho h\rangle\langle\tau_b/\rho h\rangle \approx \langle\tau_b\rangle + \langle h\rangle\langle\tau_b\rangle[\overline{\overline{h^{-1}}}(x_2) - \overline{\overline{h^{-1}}}(x_1)] + \cdots \text{ second-order terms.}$$

An estimate of the expansion error term

$$\epsilon_\tau = \langle h\rangle\langle\tau_b\rangle[\overline{\overline{h^{-1}}}(x_2) - \overline{\overline{h^{-1}}}(x_1)] = 10^3 \times 35 \times 5 \times 10^{-5} = 1.75 \text{ dyn cm}^{-2}$$

shows that for the Estuary ϵ_τ is also small compared to the second-order terms and can be neglected here. Thus our use of $\langle\tau_b\rangle$ is valid to second order.

Therefore, the first-order results from the Estuary, with finite breadth changes, are consistent with Ianniello's (1979) analysis for very small breadth variation. The second-order departures from the primary balance are due to the combined effects of the convective and the inertial accelerations [terms (c) and (b) in (27)], while the third-order departures, such as ϵ_η and ϵ_τ, are unresolved within our measurement uncertainties.

The effect of the small downstream divergence in the study area is to produce a positive definite fluctuation in the convective acceleration term $-\rho h\delta(U^2/2)/\delta x$, with a resulting bias in our estimates of the downstream bottom stress. But this is misleading because we are not able to measure the mean pressure gradient force and have removed the mean from our analyses. An estimate of the magnitude of the pressure gradient force can be made by considering Ianniello's (1979) solution of tidal flow in a breadth-variable estuary. Although his solution is strictly applicable for breadth variations that are smaller than those in the Estuary, the qualitative features of that solution should be applicable.

Ianniello finds the vertical structure of the second-order time-averaged Eulerian flow $\bar{u}_2$ and pressure gradient $\partial\overline{\eta_2}/\partial x$ from his dimensionless second-order momentum equation

$$\overline{u_1\frac{\partial u_1}{\partial x}} + \overline{w_1\frac{\partial u_1}{\partial z}} = -\frac{\partial\overline{\eta_2}}{\partial x} + \frac{1}{2}\frac{\partial}{\partial z}N\frac{\partial\overline{u_2}}{\partial z} \quad (29)$$

and the continuity equation, where the first-order flow u_1, w_1 is known and N is a constant eddy viscosity. If we assume that $u_1\partial u_1/\partial x$ is the most important convective acceleration term, then we can rewrite (29) as

$$\underbrace{\left[-\frac{\partial\overline{(u_1^2/2)}}{\partial x}\right]}_{\text{(a)}} + \underbrace{\left(-\frac{\partial\overline{\eta_2}}{\partial x}\right)}_{\text{(b)}} + \underbrace{\left(\frac{N}{2}\frac{\partial^2\overline{u_2}}{\partial z^2}\right)}_{\text{(c)}} = 0. \quad (30)$$

and consider the vertical structure of each term. In a diverging channel the convective acceleration term (a) is positive definite with a decrease with depth as shown in Fig. 11. The stress term (c) distribution can be crudely inferred from the Ianniello (1979) Eulerian residual-flow structure, which shows a near-surface flow toward $+x$ and a relatively stronger near-bottom flow toward $-x$. The stress structure shown is consistent signwise. In order for a balance to be achieved in (30) the pressure-gradient term (b), which is depth-independent, must be negative and of the same order as term (a). According to our estimates of mean convective acceleration shown in Table 1, this means that $\partial\overline{\eta_2}/\partial x$ is of order

$+10^{-5}$ (or 1 cm km^{-1}) in the study area under consideration. This compares with an rms $\partial\eta_1/\partial x$ of 4×10^{-5} for the first-order tidal motion. Thus there are significant steady tilts which might be resolved with an accurate geodetic leveling of adjacent tide-measuring stations in the study area.

b. Bottom-stress parameterization

It is common practice to relate bottom stress τ_b and current u_{100} at 100 cm above the bottom according to $\tau_b = \rho C_{100} u_{100}^2$, where ρ is the average water density and C_{100} the drag coefficient corresponding to u_{100}. In order to compare our results with others, we compute a semidiurnal-tidal time series of section-averaged values of C_{100} from the above relationship by assuming that the values of τ_b in Fig. 10 are accurate and by estimating u_{100} in accordance with the relation $u_{100} \approx 0.75 \langle U \rangle$. (The latter relation has been verified with the current profile measurements.) The results of this computation, using data shown in Fig. 10, appear in Table 2 and show that C_{100} is about an order of magnitude larger than most reported values, varies in time by more than an order of magnitude, and is asymmetric relative to the tidal current.

If one accepts the accuracy of our τ_b estimates then it is clear from Fig. 8 that the variability and asymmetry in C_{100} are related to the variability in the dynamical balances. For example, the inertial and convective-acceleration terms produce a considerable asymmetry in the ebb and flood bottom stress in contrast to the near symmetry of current velocity itself as shown in Fig. 10. Since this simple bottom-stress parameterization is based on a steady momentum balance involving a typical local flow at 100 cm elevation, it is not surprising that it is inadequate for describing hydrodynamic stress in some tidal channels, where the magnitude and phase of additional terms in the momentum balance may be important. For example, we find that the tidal mean value of C_{100} is 3.5×10^{-2}. This is about an order of magnitude larger than those found by Sternberg (1968), using a log-profile method in a few tidal channels in the northwest. The implication here is that a relatively larger mean bottom stress is required in the local Estuary to balance the characteristic mean pressure gradient. Furthermore we believe that although a significant amount of the scatter in C_{100} observed by Sternberg (1968) is due to sampling variability as pointed out by Heathershaw and Simpson (1978), some of the variability is real and due to the unsteadiness in the dynamics. In order to model residual flows due to hydrodynamic nonlinearity, it may be important to specify bottom stress in a more realistic way.

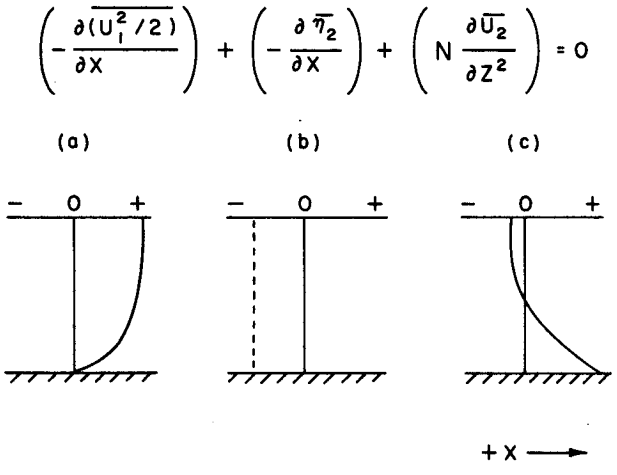

FIG. 11. Crude estimates of the vertical structure of the terms in (30) are shown. The form of (a) is found in a diverging channel with bottom friction and the form of (c) is inferred from Ianniello's (1979) solution for the Eulerian mean flow in a diverging channel. The inferred distribution of the pressure-gradient term required for a balance is shown in (b).

TABLE 2. A time series of computed drag coefficients based on bottom stress and velocity values shown in Fig. 10. The coefficients C_M and C_{100} are based on $\langle U \rangle$ and u_{100} (see text), respectively.

Time (h)	τ_b (dyn cm^{-2})	$\langle U \rangle$ (cm s^{-1})	u_{100} (cm s^{-1})	C_M	C_{100}
3	60	82	62	0.009	0.015
5	23	40	30	0.014	0.025
7	−39	−27	−20	0.052	0.095
9	−30	−97	−73	0.003	0.006
11	−30	−50	−38	0.012	0.020
13	15	20	15	0.037	0.065
15	53	70	53	0.011	0.018

c. Dissipation

Finally, we compare our dissipation results with an independent estimate. From the work of Ippen (1966) it can be shown that an alternative relation for calculating the average rate of dissipation $\bar{\phi}$ for a long wave is

$$\bar{\phi} = \int_{-h}^{0} \lambda^{-1} \int_{0}^{\lambda} \rho\nu(\partial u/\partial z)^2 dx dz,$$

where λ is the tidal wavelength and ν the kinematic viscosity. Velocity-profile data from the study site and the eddy viscosity, $\nu_e = 0.0236z - 0.00238z^2$, which was determined in accordance with the results of Swift *et al.* (1979) for the Estuary, have been used to determine $\bar{\phi} = 4800$ ergs cm^{-2} s^{-1}. This value, which is based on central-channel velocity profiles, is twice the 14-day mean value of $\langle \phi \rangle = 2478$ and therefore may provide a measure of the lateral variability of dissipation rate within the study site. Future studies including direct measurements of bottom stress will shed more light on this question.

d. *Summary of conclusions*

In this paper we demonstrate a dynamical method for inferring a space-averaged tidal bottom stress and associated energy dissipation rate for a shallow well-mixed estuary. We find a first-order dynamical balance between along-estuary pressure gradient and bottom friction, and thus sea level measurements alone may be useful in estimating dissipation for estuaries where similar dynamical conditions prevail. Because of the spatial averaging, however, we would not expect agreement between these stress estimates and those made on the basis of point measurements.

As a consequence of this approach we are able to show how instantaneous bottom-stress values depend upon a time-varying blend of contributions from the different terms in the momentum balance. In particular for this estuary a combination of the second-order inertial and convective-acceleration terms causes an asymmetry in the ebb and flood bottom stress. Under the conditions described the use of a constant drag coefficient with a depth-averaged velocity is an inaccurate way of parameterizing bottom stress.

Acknowledgments. This work was made possible with the field assistance of Ms. Karen Garrison, Mr. Andrew Silver, Mr. Ed Schmidt and the captain of the R. V. *Jere Chase*, Mr. Paul Pelletier. Dr. J. D. Irish provided valuable assistance in the data analysis phase of this work. A special thank you is reserved for Drs. M. R. Swift and R. Reichard, who provided field assistance and constructive criticism of this manuscript, and in particular to Dr. J. P. Ianniello, who provided very helpful comments on the development of some of the analysis and on an earlier manuscript.

This material is based on research supported in part by the University of New Hampshire Sea Grant 4-20379-215, the UNH Leslie Hubbard Fund, and the National Science Foundation under Grant OCE 78-26229.

REFERENCES

Arellano, E., 1978: An application of a segmented tidal prism model to the Great Bay Estuarine system. M.S. thesis, Dept. of Earth Sciences, University of New Hampshire, 79 pp.

Bowden, K. F., L. A. Fairbairn and P. Hughes, 1959: The distribution of shearing stresses in a tidal current. *Geophys. J. Roy. Astron. Soc.*, **2**, 288–305.

Garrett, C., 1975: Tides in gulfs. *Deep-Sea Res.*, **22**, 23–35.

Heathershaw, A. D., and J. H. Simpson, 1978: The sampling variability of Reynolds stress and its relation to boundary shear stress and drag coefficient measurements. *Estuarine Coast. Mar. Sci.*, **6**, 263–274.

Hendershott, M., and W. Munk, 1970: Tides. *Annual Review of Fluid Mechanics*, Vol. 2, Annual Reviews Inc., 205–224.

Ianniello, J. P., 1979: Tidally induced residual currents in estuaries of variable breadth and depth. *J. Phys. Oceanogr.*, **9**, 962–974.

Ippen, A. T., Ed., 1966: *Estuary and Coastline Hydrodynamics*. McGraw-Hill, (see Sec. 1.9), 744 pp.

Johns, B., 1978: The modeling of tidal flow in a channel using a turbulence energy closure scheme. *J. Phys. Oceanogr.*, **8**, 1042–1049.

Levine, E. R., and K. E. Kenyon, 1975: The tidal energetics of Narragansett Bay. *J. Geophys. Res.*, **80**, 1683–1688.

McLellan, H. J., 1958: Energy considerations in the Bay of Fundy system. *J. Fish. Res. Bd. Can.*, **15**, 115–134.

Miller, G. R., 1966: The flux of energy out of the deep oceans. *J. Geophys. Res.*, **71**, 2485–2489.

Silver, A., and W. S. Brown, 1979: Great Bay Estuary Field Program, 1975 data report, Part 2: Temperature, salinity and density. UNH Sea Grant Tech. Rep. UNH-SG-163, 59 pp.

Smith, J. D., and S. R. McLean, 1977: Spatially averaged flow over a wavy surface. *J. Geophys. Res.*, **82**, 1735–1746.

Sternberg, R. W., 1968: Friction factors in tidal channels with differing bed roughness. *Marine Geol.*, **6**, 243–260.

Swenson, E. M., W. S. Brown and R. Trask, 1977: Great Bay Estuary Field Program, 1975 data report, Part 1: Currents and sea level. UNH Sea Grant Tech. Rep. UNH-SG-157, 109 pp.

Swift, M. R., R. Reichard and B. Celikkol, 1979: Stress and tidal current in a well-mixed estuary. *J. Hydraul. Div. ASCE*, **105**(HY7), 785–799.

Taylor, G. I., 1919: Tidal friction in the Irish Sea. *Phil. Trans. Roy. Soc. London*, **A220**, 1–93.

Trask, R. P., and W. S. Brown, 1979: A study of estuarine bottom stress. UNH Sea Grant Tech. Rep. UNH-SG-166, 63 pp.